Webology (ISSN: 1735-188X)
Volume 18, Number 6, 2021

Impact Of Charge Interaction, H-Bonding Elucidations By Structural And Biological Activity Of Diammonium Hydrogen Orthophosphate

G.Bagavathi Sankar[1] , D.Usha[2]

[1]Reg.No18223282131003, Department of Physics, St.Johns College of Arts and Science Ammandivilai

[2]Associate Professor, Department of Physics, Womens Christian College, Nagercoil-629001

[1,2]Affiliated to Manonmaniam Sundaranar University, Abishekapatti, Tirunelveli-627 012, Tamilnadu, India

Abstract

The structure-activity of diammonium hydrogen orthophosphate optimized using the density functional theory method using B3PW91/6-31++G (d, p) set. Hydrogen bonding interactions confirmed by Natural Bonding orbitals (NBO) Analysis. The frontier molecular orbital analysis provided a electron transport in the molecule. The most reactive site of the molecules was predicted by the molecular electrostatic potential map and also natural charge analysis. Vibrational spectral assignments predicted the aid of Normal Coordinate Analysis. Antimicrobial activity performed for biological activity screening of the molecules along with drug likness confirmed its antibacterial activity.

Keywords: Antibacterial; drug likeness; FT IR; Raman; ELF; LOL.

1. Introduction

In recent years, materials focused on phosphates and ammonium has been significantly innovative. These compounds are established to be fascinating in numerous fields of applications for instance biotechno logical, biology, and bioactive ceramics materials [1-4]. Diammonium phosphate is used

for fireproofing textiles, paper, wood and vegetable fibers, and used in purifying sugar, in yeast cultures, in dentifrices, in corrosion inhibitors and also widely used in fertilizers. Phosphates play an important role in living and non living nature and the properties of phosphate ions are crucial in many areas of science and technology. Diammonium Hydrogen Orthophosphate(DAP) is a bioactive material. An overview of the literary works uncovers that there has been no thorough experimental and theoretical exploration of DAP. In order to better realize the structure-activity relationship, vibrational spectroscopic techniques, and biological activity performed. DFT computation was performed at B3PW91/6-31++G(d,p) method using Gaussian'09 program to optimize the structure. The natural bond orbital (NBO) analysis of DAP has been calculated to analyze the stabilization and intra and inter-molecular charge transfer interactions. HOMO-LUMO energy gap was used to understand the biological activity of DAP. Molecular electrostatic potential (MEP), ELF, LOL and RDG methodologies have been extensively applied to classify and understand the hydrogen bonding interactions. Herein work, the determinations have been occupied to expect the thorough depiction of the molecular geometry, vibrational frequencies, NBO analysis, hydrogen bonding interaction and antibacterial activity of DAP. In order to take into the account, the effect of intermolecular interaction on geometrical parameters and spectroscopic analysis to the gathering construct up and the molecule is associated in N-H…O hydrogen bonding and resonance effect.

2. Experimental Details

FTIR absorbance spectrum using KBr pellet method with resolution of 1.0 cm^{-1} using Perkin Elmer Spectrometer. FT Raman spectrum was recorded with BRUKER RFS 27: Stand alone FT Raman Spectrometer and the laser source used was Nd: YAG 1064 nm with spectral resolution of 2.0 cm^{-1}. UV-VIS absorption spectrum of DAP in water as a solvent is scrutinized in the range 200-800 nm with spectral Bandwidth 2nm using UV-VIS spectrophotometer. The antimicrobial activity of DAP was screened by agar well diffusion method.

3. Computational Details

Quantum chemical design has been executed using B3PW91/6-31++G(d,p) basis set by the Gaussian '09 program [5]. MOLVIB program written by Sundius [6,7] lets a least- squares enhancement of multiple scale factors of the QM force field in addition calculation of the normal modes[8, 9]. UV-vis spectra, electronic transitions, excitation energies, absorbance and oscillator strengths were calculated with the time-dependent DFT method[13-16]. Natural bond orbital (NBO) analysis were executed using NBO 3.1 program [17]. The illustrative suggestion of the intermolecular interactions collected from the ELF, LOL, RDG properties were achieved using multiwfn multifunctional wave function analyser [18,19] and plotted with VMD molecular visualisation program [20].

4. Results and Discussion

4.1 Structural Analysis

Details regarding bond lengths and bond angles and dihedral angles of DAP molecule are given in Table 1 and the optimized structure is given in Fig.1.

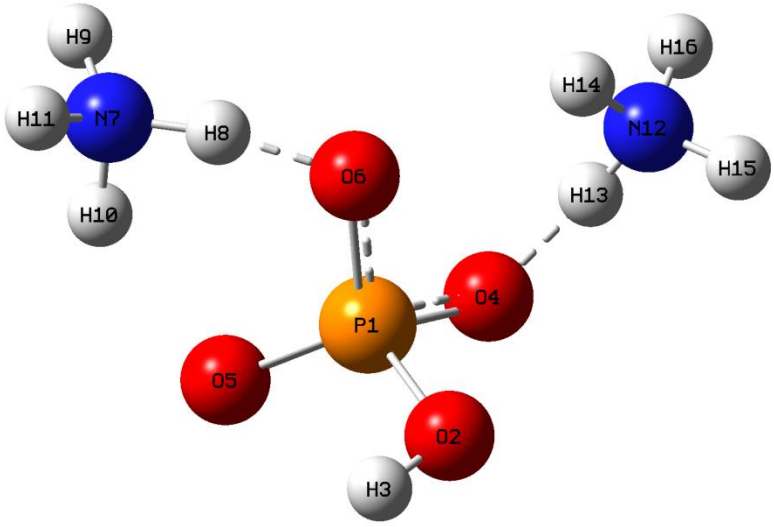

Fig 1 Optimized structure of DAP

From Table 1, the P-O bond distances differ from 1.486 to 1.646 Å, O-P-O bond angles vary from 101° to 116° indicates the distortion of P-O group. The exploration of bond lengths and angles confirm P-O is distorted from normal bonds. The P-O bond distances explicitly support the ascription of hydrogen atoms covalently connected to O2, O4, and O6 and these bond lengths are 1.62-1.64Å among these P1-O4 and P1-O6 are higher than other P1-O2 which confirms P1-O4 and P1-O6 are involved in the hydrogen bonding interaction. P-O bond distances in the P1-O2 , P1-O4 and P1-O6 are self-consistent when H is covalently bonded to the oxygen and bond length of P1-O5 is 1.489 Å where there is not any covalently bonded hydrogen atom and there is no hydrogen bonding interaction. Intermolecular N-H…O hydrogen bonding interactions have been showing by intermolecular links with H…O bond distances O4…H13 and O6…H8 are 1.399Å and 1.325Å, which are substantially shorter than van der Waals separation between O with H atom (2.72˚A), which is important to get a closer insight into these interactions and design molecules with improved biological profile[21].

Table 1 Optimized Parameters of DAP

Bond length	(Å)	Bond Angle	(°)	Dihedral Angle	(°)
P1-O2	1.6241	O2-P1-O4	102.0389	O4-P1-O2-O3	-159.7844
P1-O4	1.5763	O2-P1-O5	113.4506	O5-P1-O2-O3	-33.6795
P1-O5	1.4896	O2-P1-O6	104.2104	O6-P1-O2-O3	90.1925

P1-O6	1.6062	O4-P1-O5	116.4681	O2-P1-O4-H13	-79.2765
O2-H3	0.9654	O4-P1-O6	105.8679	O5-P1-O4-H13	156.6169
O4-H13	1.6517	O5-P1-O6	113.4512	O6-P1-O4-H13	29.4814
O6-H8	1.6631	P1-O2-O3	110.7709	O2-P1-O6-H8	-132.0341
N7-H8	1.0200	P1-O4-H13	171.7365	O4-P1-O6-H8	120.7684
N7-H9	1.0149	P1-O6-H8	165.0307	O5-P1-O6-H8	-8.1625
N7-H10	1.0228	H8-N7-H9	118.2446	P1-O4-13-N12	-14.4527
N7-H11	1.0149	H8-N7-H10	93.3798	P1-O6-H8-N7	3.4957
N12-H13	1.0184	H8-N7-H11	118.3073	H9-N7-H8-O6	-112.3127
N12-H14	1.0174	H9-N7-H10	108.5206	H10-N7-H8-O6	0.8243
N12-H15	1.0152	H9-N7-H11	108.0451	H11-N7-H8-O6	114.1575
N12-H16	1.015	H10-N7-H11	108.6721	H14-N12-H13-O4	-5.9687
		O6-H8-N7	109.5835	H15-N12-H13-O4	109.8593
		H13-N12-H14	100.8869	H16-N12-H13-O4	-122.9718
		H13-N12-H15	114.3155		
		H13-N12-H16	116.2467		
		H14-N12-H15	108.1863		
		H14-N12-H16	108.4436		
		H15-N12-H16	108.1624		
		O4-N13-N12	113.4938		

4.2 Bonding Analysis

NBO analysis explicates the stabilization of system, molecular bonding, hyper conjugative interactions, and charge transfer [22–25] and the stabilization energy listed in Table 2. The hyper conjugative interaction LP (3) of O6 to σ*(N7-H8) is the strongest hydrogen bonding interaction with the energy 107.79 kcal/mol. Some strongest interaction also can be seen in the Table 2 which are for LP (3) of O4 to σ*(N12-H13) and LP (1) of O6 to σ*(N7-H8) are 65 kcal/mol and 13 kcal/mol respectively. These interactions show the good stabilization energy between lone pairs and σ anti-bonding orbital. This stabilization of DAP is confirmed by intermolecular charge transfer between phosphate groups to ammonium group and also n→σ* interactions.

Table 2 Bonding Analysis of DAP

Donor (i)	**Acceptor (j)**	**E(2)[a] (kcal/mol)**	**E(j)-E(i)[b] (a.u)**	**F(ij)[c] (a.u)**
LP(3)O5	N7-H10	10.40	0.64	0.075
LP(1)O5	N7-H10	2.48	1.08	0.046
LP(1)O6	N7-H8	13.24	1.12	0.112

LP(2)O6	N7-H8	0.13	0.76	0.009
LP(2)O6	N7-H11	0.16	0.65	0.009
LP(2)O6	N7-H9	0.24	0.65	0.011
LP(3)O6	N7-H8	107.79	0.86	0.275
LP(3)O4	N12-H13	65.28	1.09	0.054
LP(1)O6	N12-H14	1.51	0.99	0.03
LP(3)O4	N12-H16	0.19	0.65	0.010
LP(3)O4	N12-H15	0.09	0.65	0.007
LP(2)O6	N12-H14	1.28	0.63	0.026

4.3 Vibrational Analysis

The vibrational spectral assignments have been performed by NCA using the scaled quantum mechanical force field methodology. The simulated and experimental FT-IR along with FT-Raman spectra are publicized in Fig. 2 and 3 respectively. The thorough vibrational assignments with PED contributions are presented in Table 3. The detailed vibrations of NTE are given below:

4.3.1 Ammonium Vibration

NH_3^+ asymmetric and symmetric stretching bands assigned in the region 3330 and 3080 cm^{-1} respectively [26]. The asymmetric stretching is observed in IR at 3375 cm^{-1} and 3300 cm^{-1} and the scaled values are 3350 cm^{-1} and 3313 cm^{-1}. The symmetric stretching is observed in IR at 3338 cm^{-1}, 3330 cm^{-1} and 3257 cm^{-1} and in Raman at 3330 cm^{-1} and 3313 cm^{-1} which are good agreement with the scaled values as given in Table . The red shift in NH stretching wavenumber indicates the formation of intermolecular N-H…O hydrogen bonding of the ammonium ion with phosphate group. N-H…O bond distances in optimized structure and natural bonding orbital supports the existence of N-H…O hydrogen bonds in the molecule. The NH asymmetric deformation vibrations usually appear in the region 1660–1610 cm-1 and the symmetric deformation in the region 1550–1485 cm-1 [27]. Strong intensity peak in IR at 1662 cm^{-1} and at 1622 cm^{-1} are assigned asymmetric deformation and symmetric bending vibration which excellent agreement with scaled values.

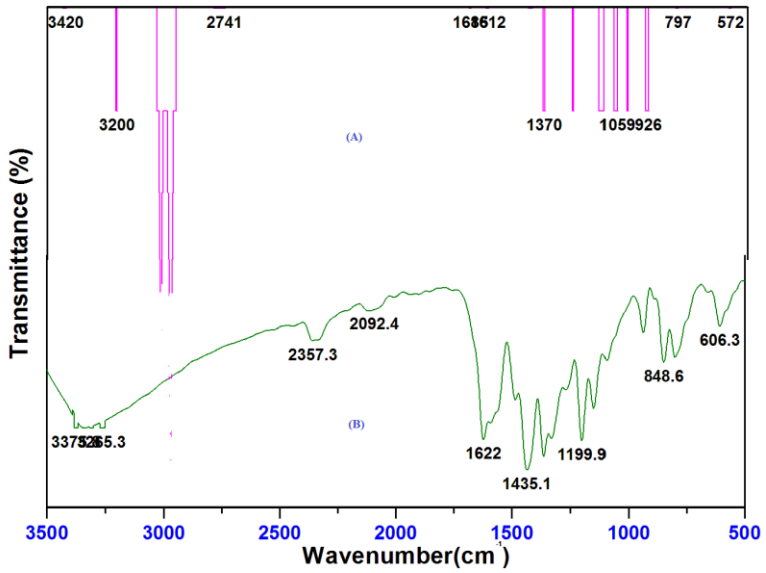

Fig 2 FT IR spectra

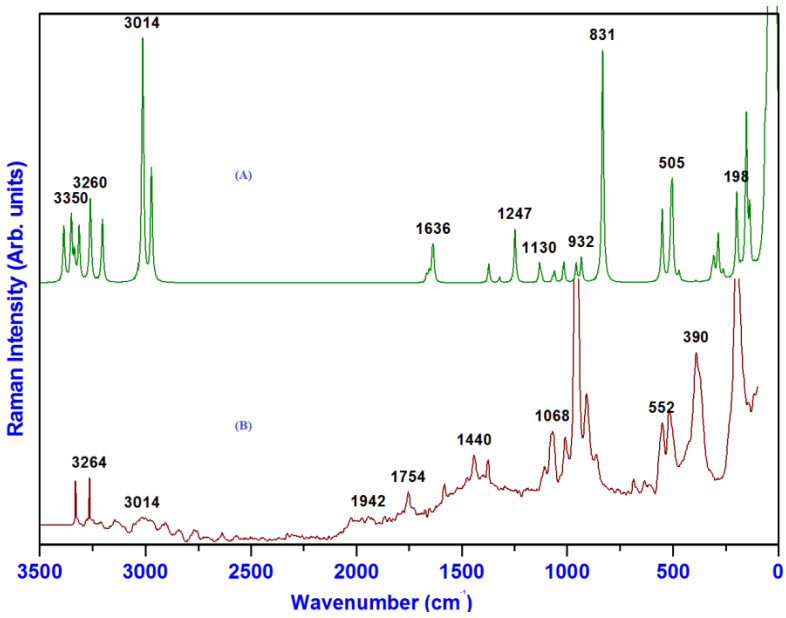

Fig 3 FT Raman spectra

4.3.2 Phosphate Vibration

Important vibrational modes of DAP is the free orthophosphate ion $[PO4]^{3-}$ antisymmetric stretching, symmetric stretching, antisymmetric bending, symmetric bending modes appear at 1017 cm^{-1}, 938 cm^{-1}, 567 cm^{-1} and 420 cm^{-1} respectively [35]. Antisymmetric stretching vibration of DAP is observed in IR at 958 cm^{-1} as a strong band and as a medium band in Raman at 1008 cm^{-1}. Symmetric stretching vibration of DAP is observed as a strong in IR at 937 and 848 cm^{-1}.

Antisymmetric and symmetric bending vibration of DAP are observed as a strong band in Raman at 552 cm^{-1}. All these values are good agreement with scaled values which are given in Table.

Hydroxyl group Vibration

Generally, O-H stretching vibration is characterized by broad bands around 3400–3500 cm^{-1}[28] and it has been observed as a broad shoulder band at 3385 cm^{-1} in IR with pure 100% PED contributions good agreement by scaled at 3385 cm^{-1} which is red shifting owing to inter- then intra-molecular hydrogen bonding effect. Bending vibration is observed in IR at as a strong band at 1363 cm^{-1} and the scaled value at 1371 cm^{-1}.

Table 3: Vibrational assignment of DAP by NCA based on SQMFF calculations

Observed fundamentals/cm^{-1}		**Selective scaled B3LYP/6-31G(d) force field**	
ν_{IR}	**ν_{Raman}**	**Cal cm^{-1}**	**Assignment with PED (≥10%)**
3385sh		3385	υOH(100)
3375sh		3350	υAMOS(98)
3338s		3350	υAMIS(96)
3330sh	3330s	3334	υAMIS(73), AMOS(27)
3300sh		3313	υAMOS(53), υAMSS(28), AMIS(19)
3257s	3264s	3260	υAMSS(68), υAMOS(22), AMIS(8)
		3202	υAMSS(96)
	3014s	3014	υOHB (92),
		2972	υOHB (92),
1662s		1667	υAMIB(80), υAMOB(19)
		1654	υAMIB(76), υAMOB(24)
		1639	υAMOB(71), υAMIB(24)
1622s		1634	υAMOB(79), υAMIB(19)
1363s		1371	βOHB(68), TBOHB (10), TAM (10)
		1320	βOHB(74), υPO (12)
		1247	υPO(65), βOHB(25)
		1130	βAMSD(92)
	1106w	1121	AMSD(90)
	1068s	1069	τBOHB (51), τAM (45)
		1060	τBOHB (52), τAM (43)
	1008m	1016	υPO(42), τBOHB (21), τAM (18), βOH (12)
958s		957	βOH (57), υPO(32)

937s		932	υPO(92)
848s		831	υPO(66), BOH (11), POSD(8)
	552s	552	POOB(42), POSD(12), AMOR(11),
		509	POSD(59), POOB(11), PO(8),
		504	POIB(65), υNH(11), POSD(8),
		471	BOHB(36), AMOR(26), POOB(17), AMIR(9)
	390s	391	AMIR(46), BOHB(24), POIB(10),
		315	τBOHB (47), τAM (40), AMOR(9)
		311	τBOHB (51), τAM (32), AMIR(9)
		306	υNH(40), τBOHB (22), τAM (14),
		285	τOH (23), NH(22), POIR(17), TAM (9),
		261	τNH(73), OHB (9)
	200s	198	POIR(44), POOR(24), POIB(10), τBOHB (9)
		177	τAM (64), AMIR(14), AMOR(8),
		152	TOH (27), TAM (16), TBOHB (13), POOR(10), POIR(10),
		136	BOHB(23), POOR(17), TAM (16), TBOHB (14), TOH (14),
		111	TAM (68), AMOR(17),
		63	BOHB(54), AMIR(17), TAM (14)
		44	TPO (44), TBOHB (24), TOH (10),
		22	TPO (64), TBOHB (23),

*vw-very weak; w-weak; m-medium; vs-very strong; s-strong;*ν*-stretching; SS- symmetric stretching; AS- asymmetric stretching; IP- in-plane stretching; OP- out of plane stretching; TD-trigonal deformation; AD- asymmetric deformation; ADO-out of plane asymmetric deformation; PU- Puckering; AT-asymmetric torsion; ATO-out-of plane asymmetric torsion; R-ring; NI- nitro;* ρ - Rocking; δ-*Scissoring;*.

4.4 FMO analysis

HOMO LUMO plots as well as DOS plots are given in Fig. Frontier molecular orbital (FMOs) energy plays a crucial role in chemical stability. The HOMO is located over the phosphate group and LUMO is located over the ammonium group also reveals that the adsorption of molecule interrupts the HOMO and LUMO distribution. HOMO energy is - 6.353918 eV and LUMO energy is -0.365177 eV and the energy difference between the frontier molecular orbitals (FMO's) is 5.988741eV. This shows that DAP has small FMOs energy gap due to the greater extent of molecular charge transfer of this system. Low energy gap molecules improve the molecular electrical transport properties and biological activity.

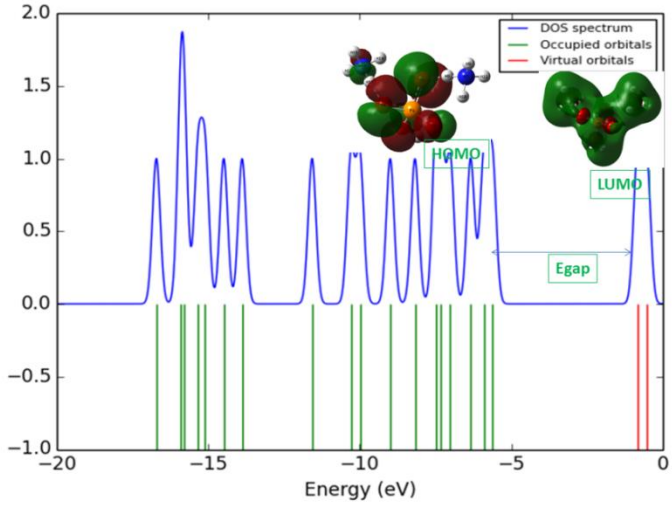

Fig 4 DOS plot with HOMO LUMO plot

4.5 UV vis Spectral Analysis

To acquire the electronic transitions of DAP molecules, TD-DFT calculations were implemented and results are tabulated in Table 4 and the UV spectrum also given in figure 4. The molecular absorption of DAP are 238, 270 nm and 433 nm and the theoretical values also good agreement with experimental. These absorption peaks are due to the charge transfer interaction between a lone pair of electrons present in the oxygen atoms of phosphate group to antibonding σ electrons in the ammonium group and this absorption bands of the molecules is assigned to the n→σ* [29] which are responsible for the enhanced activity of the molecule. The optical band gap has been obtained from absorption spectrum and the DOS plot (figure 6) is around 5eV and their contributions is H-2 to LUMO with 93%. The energy required for exciting electrons from n → σ* transition states is found at 5.9 eV which is consistent with the calculated frontier molecular orbital energy gap.

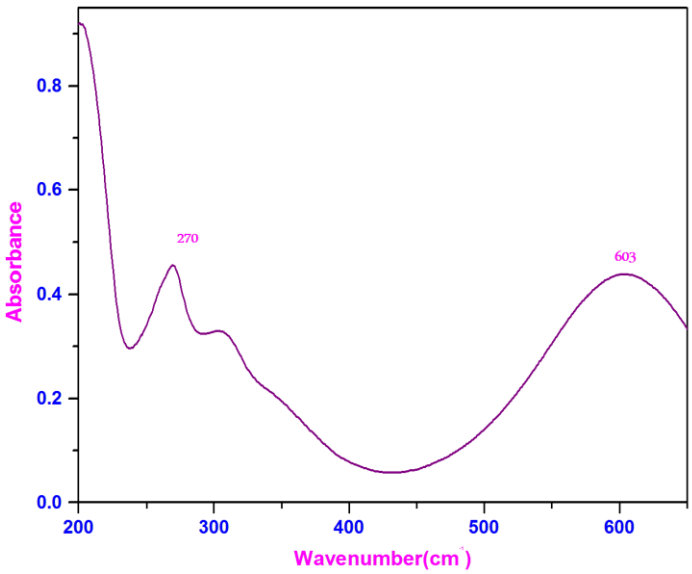

Fig 6 UV vis spectrum

Table 5 UV-vis wavelength and their contributions of DAP

Energy (cm^{-1})	Experimental		Theoretical		Osc. Strength	Symmetry	Major contributions
	Wavelength (nm)	Bandgap	Wavelength (nm)	Bandgap			
32920.	433	2.8637	303	4.0924	0.0066	Singlet-A	HOMO→LUMO (99%
35139.			284	4.3661	0.0028	Singlet-A	H-1→LUMO (98%)
36142.	270	4.5925	276	4.4927	0.005	Singlet-A	HOMO→L+1 (99%)
38553.			259	4.7876	0.0021	Singlet-A	H-1→L+1 (96%)
39432	238	5.2100	233	5.3218	0.0077	Singlet-A	H-2→LUMO (93%)

4.6 Charge Analysis

4.6.1 Molecular Electrostatic Potential Analysis

MEP is a noble director in evaluating the molecular interaction with its neighboring [31] and also provides a pictorial understanding of shape, size, charge density and relative polarity of the molecule [32]. This 3D mapping supports to localize the reactive site of the molecule by understanding the color codes. The color code initiates from red which symbolizes the highest

negative potential sites and ends with blue color which signifies the highest positive sites, in between green color signifies the site which is having a zero potential. To predict the molecular reactive sites, MEP map for DAP is given in Fig. From MEP pictorial representation, the negative potential region localizes over the phosphate group and the hydrogen atom attached to oxygen atom in the phosphate group possesses the concentrated explosion of positive charge. The delocalization of the electrons from the phosphate group into ammonium group visualize by the yellowish color which confirm the intermolecular hydrogen bonding interaction and the phosphate group show electronegative potential and higher biological activity.

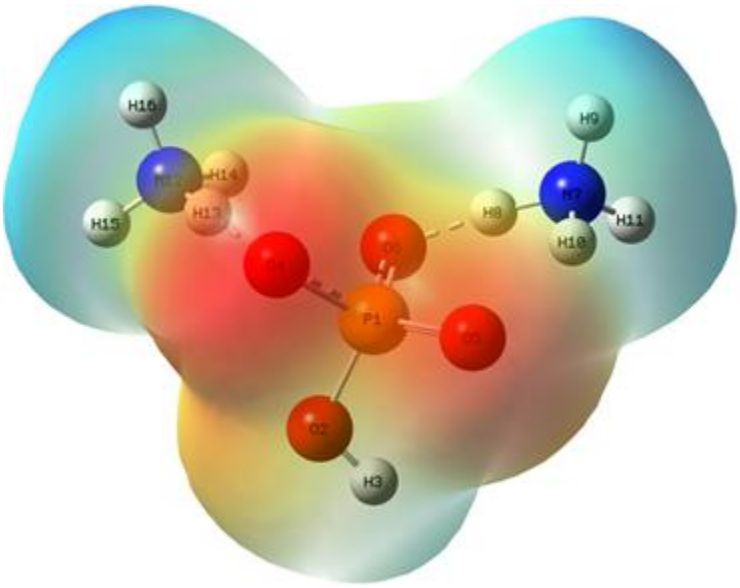

Fig 7 Molecular Electrostatic Potential

4.6.2 Natural Charge Analysis

The atomic charges were calculated Natural charge analysis. The charge value of each atom is graphically exhibited in Fig.8 . From the plot, the phosphorus has a strongest positive charge owing to this is the neighboring four oxygen atoms have substantial electronegative properties. Likewise, the oxygen atoms O4 and O6 of phosphate group shows the lowest negative charge is due the presence of charge transfer to hydrogen bond from phosphate group which confirms N-H… O hydrogen bonding interaction.

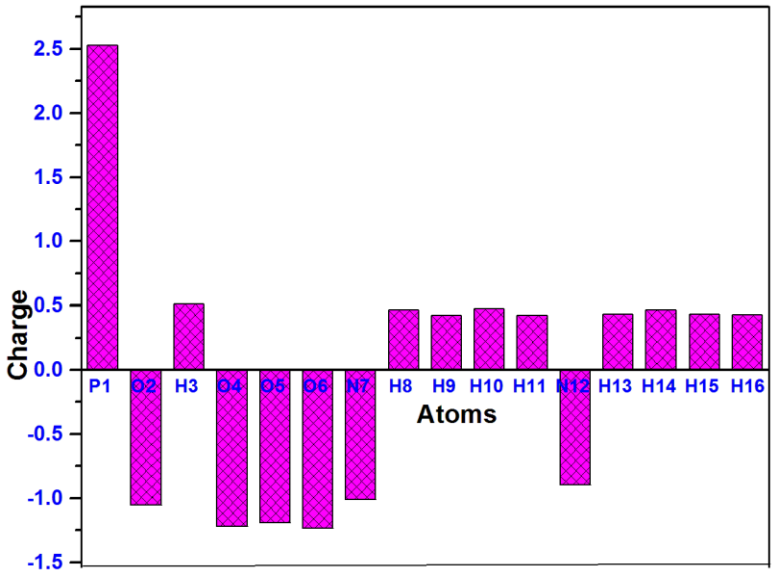

Fig.8 Natural Charge Analysis

4.7 ELF and LOL Analysis

2D Electron localization Function (ELF) and localized local maps (LOL) with color filled map representation for DAP is given in Fig. 9. ELF and LOL can be used to examine electron localization and localized electron cloud respectively [33]. From Fig. 3, the high ELF value with red colour on hydrogen atom denotes localised bonding in addition non-bonding electrons with maximum Pauli repulsion. Delocalised electron cloud is all over the molecule the all the hydrogen and nitrogen atoms shown with blue colour circle at low ELF values. The white colour present at the central part of hydrogen atom indicates the electron density is higher. The covalent region between all N-H indicated by red colour.

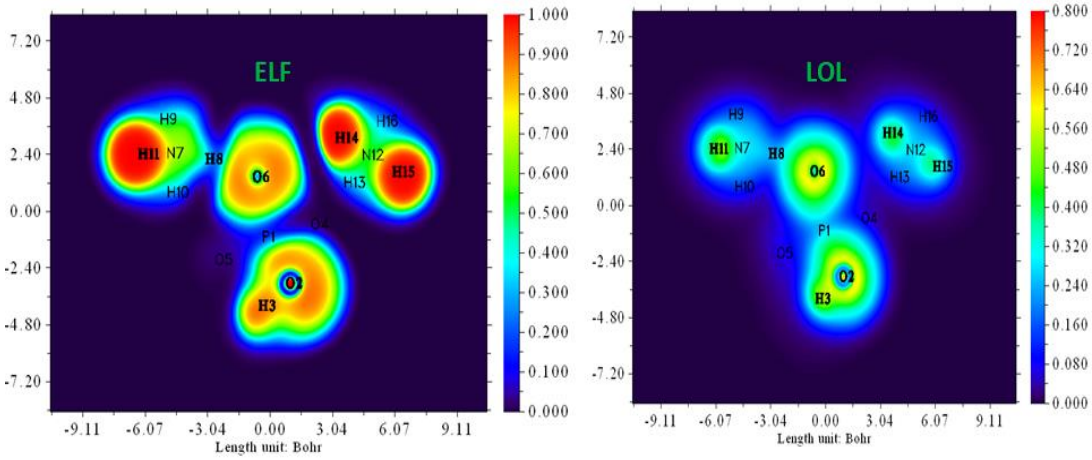

Fig 9 ELF and LOL maps

4.8 RDG Scatter Analysis

RDG study is exploring the non-covalent interactions present in the molecule. This technique is considerable useful to study low interactions, van der Walls interaction, steric effect (exactly repulsive interaction) within the molecule. The pattern of electron density against Eigen value second large λ2 (Hessian matrix) is in authority to elucidate the various non-covalent interactions. Negative, positive (highlighted with red colour) and very low or almost equal to zero values (highlighted with green colour) of λ2 are assigned for high density, steric effect and Vander Walls interactions respectively. The existence of a hydrogen bond is signposted by the blue colour in the Fig. 10.

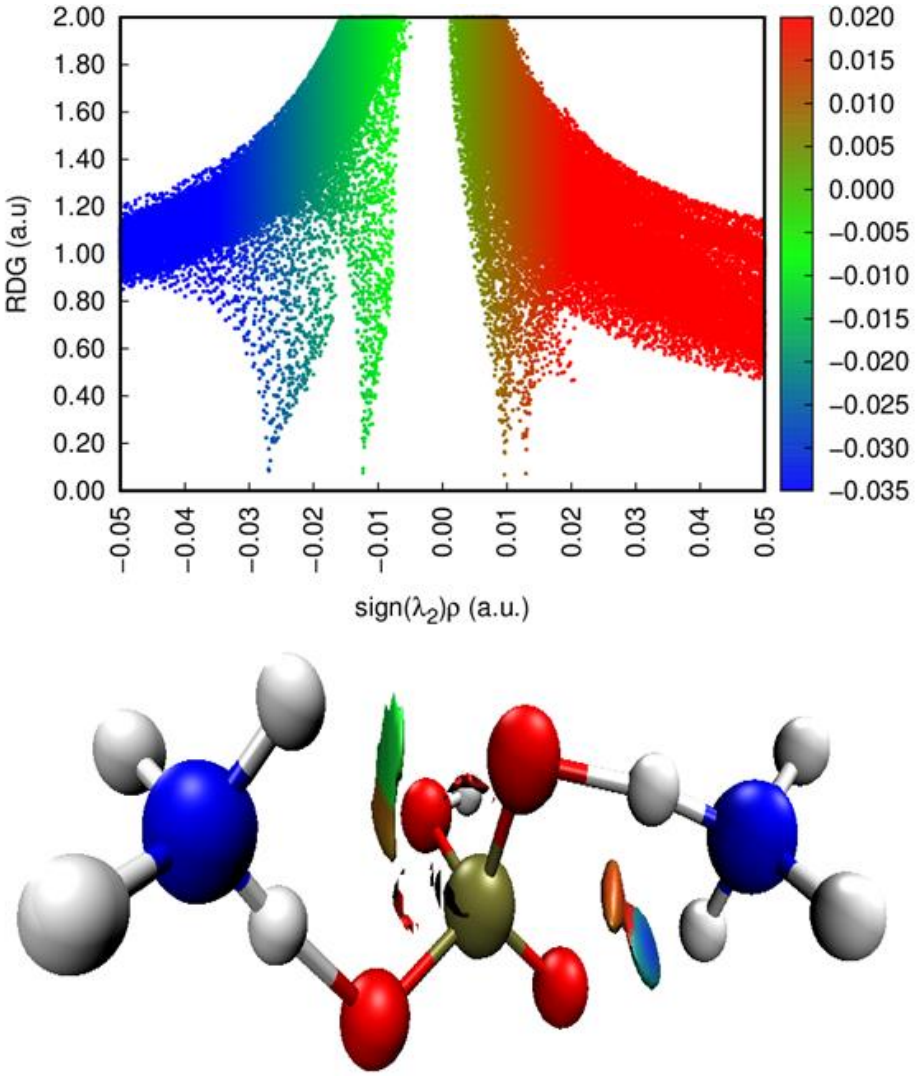

Fig . 10 RDG Analysis

4.9 Antimicrobial Activity

The DAP molecule was screened for its in vitro antimicrobial activity against bacterial and fungal strains by agar well diffusion method and it was tested against four human pathogenic

microorganisms were observed and the diameter of the inhibition zone diameter values (mm) was measured around the well. The activity was determined by measuring the inhibition zone of the investigated compound. The antimicrobial activity test for microbial strains were measured and mentioned in the Table 7 and the photographed are shown in Figure 11. Antimicrobial activity against human pathogens of clinical isolates (*Escherichia coli, Bacillus cereus, Staphylococcus aureus, Streptococcus pyogenes and Klebsiella pneumonia*). NTE showed a maximum inhibition of zone diameter 15mm by *K Streptococcus pneumoniae*. This is followed by *Bacillus cereus* and *Klebsiella pneumoniae* with a diameter shows resistant to NTE. No inhibition zone is formed in *Escherichia coli* . *Streptococcus pneumoniae* can be treated with antibiotics. These results clearly indicate that the compound has antibacterial activities against the tested organisms.

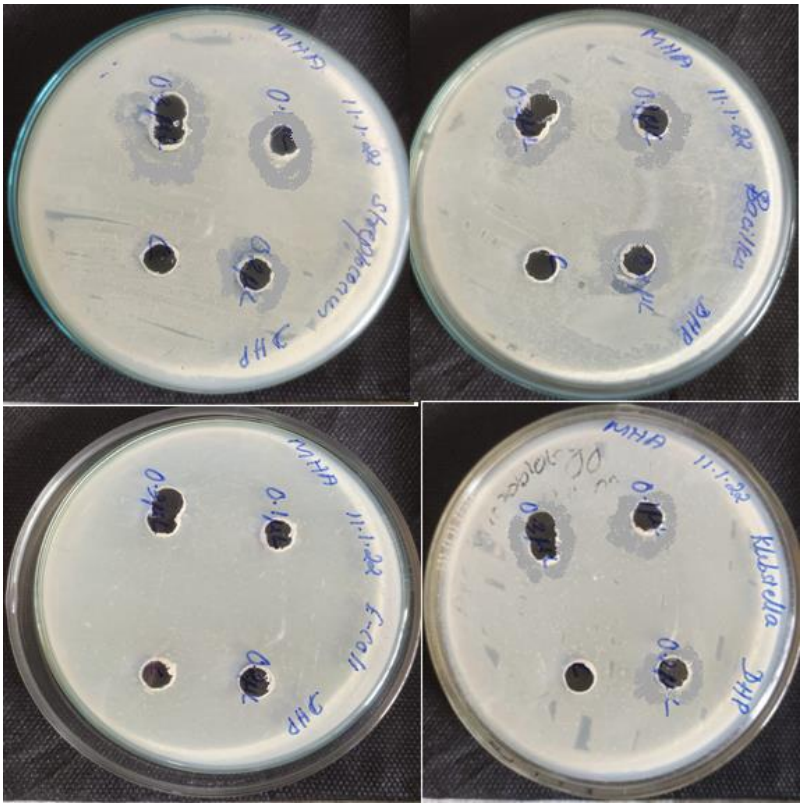

Fig 11 Antimicrobial activity of DAP

Table 8 Antimicrobial activity of DHP

Bacterial pathogens	**Zone of inhibition(mm)**		
	0.1µL	**0.2 µL**	**0.3µL**
Escherichia coli	-	-	-
Bacillus cereus	12	11	10
Streptococcus pneumoniae	7	11	15

Klebsiellapneumoniae	8	10	14

4.10 Drug likeness

Drug likeness is a active balancing act of various molecular properties and structure features that determines how well a molecule has evolved into a potential drug. For a molecule to be considered a potential drug, its drug resemblance must be compatible with Lipinski's rule of five [34-35]. The label molecule's drug likeness had also been predicted and displayed in Table 9. It has been found that the factors concerned involved numbers that are multiples of five: a molecular weight less than 500; hydrogen bond donor (HBD) groups is less than 5; hydrogen bond acceptor groups and calculated log P value also accept. And so DAP has been agreed through Lipinski's rule of five and the primary and significant results in sustenance of the compound suitable a drug is determined utilizing distinct drug likeness.

Table 9 Drug likeness parameters calculated for DAP

Descriptors	Calculated	Expected
Molecular mass(Dalton)	132	<500
Hydrogen bond donor	9	<5
Hydrogen bond acceptor	4	<10
Log P	-4.3790	<5
Molar refractivity	48	40-130

4. Conclusion

Quantum chemical calculations executed using B3PW91/6-31++G(d,p) basis set. Frtom optimized structural analysis Intermolecular N-H…O hydrogen bonding interactions have been confirmed to get a closer insight into drug design molecules with improved biological profile. FT-IR and FT-Raman spectra are recorded and the detailed vibrational band assignments are performed using NCA. The red shift in NH stretching wavenumber specifies the formation of intermolecular N-H…O hydrogen bonding. FMOs energy gap confirms greater extent of molecular charge transfer of this system and improve the molecular electrical transport properties and biological activity. In NBO analysis, the non-bonded interaction lone pair with anti-bonding found to have high stabilization energy. The molecular properties related to bioavailability have been confirmed by antimicrobial activity usin agar well diffusion method. Based on the obtained results of biological parameters, Lipinski rule confirms the oral bioavailability of the title compounds. The drug likeness results proves the medicinal nature of DAP.

References

[1] Dorozhkin, S. V. Biphasic, triphasic and multiphasic calcium orthophosphates. Acta Biomater 2012, 8, 963-977, https://doi.org/10.1016/j.actbio.2011.09.003.

[2] I. A. Neacsu, L. V. Arsenie, R. Trusca, I. L. Ardelean, N. Mihailescu, I. N. Mihailescu, C. Ristoscu, C. Bleotu, A. Ficai, and E. Andronescu, Biomimetic Collagen/Zn(2+)-Substituted Calcium Phosphate Composite Coatings on Titanium Substrates as Prospective Bioactive Layer for Implants: A Comparative Study Spin Coating vs. MAPLE. Nanomaterials 2019, 9, 692, https://doi.org/10.3390/nano9050692.

[3] Hench, L. L.; Hench, J.W.; Greeenspan, D. C. Bioglass: a short history and bibliography. J. Aust. Ceram.Soc 2004, 40, 1–42, https://doi.org/10.1007/978-94-011-0541-5_1.

[4]. LeGeros, R. Z. Calcium Phosphate-Based Osteoinductive Materials. Chem. Rev 2008, 108, 4742-4753, https://doi.org/10.1021/cr800427g

[5] M.J. Frisch, G.W. Trucks, H.B. Schlegel, G.E. Scuseria, M.A. Robb, J.R. Cheeseman, G. Scalmani, V. Barone, B. Mennucci, G.A. Petersson,H. Nakatsuji, M. Caricato, X. Li, H.P. Hratchian, A.F. Izmaylov, J. Bloino,G. Zheng, J.L. Sonnenberg, M. Hada, M. Ehara, K. Toyota, R. Fukuda,J. Hasegawa, M. Ishida, T. Nakajima, Y. Honda, O. Kitao, H. Nakai, T. Vreven,J.A. Montgomery Jr., J.E. Peralta, F. Ogliaro, M. Bearpark, J.J. Heyd, E. Brothers,K.N. Kudin, V.N. Staroverov, T. Keith, R. Kobayashi, J. Normand,K. Raghavachari, A. Rendell, J.C. Burant, S.S. Iyengar, J. Tomasi, M. Cossi,N. Rega, J.M. Millam, M. Klene, J.E. Knox, J.B. Cross, V. Bakken, C. Adamo,J. Jaramillo, R. Gomperts, R.E. Stratmann, O. Yazyev, A.J. Austin, R. Cammi,C. Pomelli, J.W. Ochterski, R.L. Martin, K. Morokuma, V.G. Zakrzewski,G.A. Voth, P. Salvador, J.J. Dannenberg, S. Dapprich, A.D. Daniels, O. Farkas, J.B. Foresman, J.V. Ortiz, J. Cioslowski, D.J. Fox, Gaussian 09, Revision C.02,Gaussian Inc., Wallingford CT, 2010

[6] T. Sundius , Molvib-A flexible program for force field calculations, J. Mol. Struct. (1990) 218 ,321 .

[7] T. Sundius , Vib. Spectrosc. 29 (2002) 89e95 .

[8] G. Rauhut, P. Pulay, J. Phys. Chem. 99 (1995) 3093–3100.

[12] P. Pulay, G. Fogarasi, G. Pongor, J.E. Boggs, A. Vargha, Combination of theoretical ab initio and experimental information to obtain reliable harmonic force constants, J. Am. Chem. Soc. 105 (1983) 7037, https://doi.org/10.1021/ja00362a005.
[13] E. Runge, E.K.U. Gross, Phys. Rev. Lett. 52 (1984) 997–1000.

[14] M. Petersilka, U.J. Gossmann, E.K.U. Gross, Phys. Rev. Lett. 76 (1966) 1212–

1215.

[15] R. Bauernschmitt, R. Ahlrichs, Chem. Phys. Lett. 256 (1996) 454–464.

[16] C. Jamorski, M.E. Casida, D.R. Salahub, J. Chem. Phys. 104 (1996) 5134–5147

[17] E.D. Glendening, A.E. Reed, J.E. Carpenter, F.Weinhold, NBO Version 3.1, TCI, University of Wisconsin, Madison, 1998.
[18] T. Lu, F. Chen, Multiwfn: a multifunctional wave function analyser, J. Comput. Chem. 33 (2012) 580-592.
[19] B. Fathima Rizwana, J. Christian Prasanaa, S. Muthu, Christina Susan Abraham, Comp. Biology and Chemistry 78 (2019) 9–17,
[20] W. Humphrey, A. Dalke, K. Schulten, VMD: visual molecular dynamics. J. Mol. Graph. 14(1996) 33–38.
[21] T. Joselin Beaula, P. Muthuraja, M. Dhandapani, I. Hubert Joe, V.K. Rastogi,V. Bena Jothy, Chemical Physics Letters 645 (2016) 59–70

[22] S. Muthu , E.I. Paulraj , Solid State Sci. 14 (4) (2012) 476–487 .

[23] P. Rajesh , P. Kandan , S. Sathish , A. Manikandan , S. Gunasekaran , S. Bala Abi- rami , J. Mol. Struct. 1137 (2017) 277–291 .

[24] M. Raja , R.R. Muhamed , S. Muthu , M. Suresh , J. Mol. Struct. 1141 (2017) 284–298 . [25] J. Jayabharathi , V. Thanikachalam , F. Jayamoorthy , M.V. Perumal ,Spectrachim- ica Acta 97 (2012) 131–136 .

[38] N.R. Rajagopalan , P. Krishnamoorthy , K. Jayamoorthy , M. Austeria , J. Mod. Sci. 2 (4) (2016) 219–225 .

[26] L.J. Bellamy, The Infrared Spectra of Complex Molecules, John Wiley and Sons Inc, New York, 1975.
[31] R.M. Silverstein, G.C. Bassler, T.C. Morrill, Spectrometric Identification of Organic Compounds, John Wiley and Sons, New York, 2003.
.
[27] R. Essehli, B.E. Bali, S. Benmokhtar, H. Fuess, I. Svoboda, S. Obbade. J. Alloys Compd, 493, 654 (2010).
Oh

[28] B.C. Smith, Infrared Spectral Interpretation, A Systematic Approach, CRC Press,Washington, DC, 1999.

[29] D. S. Yadav, Organic Spectroscopy, Springer Netherlands, 2005.

[30] I. Rozas , I. Alkorta , J. Elguero , Behavior of Ylides containing N, O, And C atoms as hydrogen bond acceptors, J. Am. Chem. Soc. 122 (20 0 0) 11154–11161 .

[32] S.B. Gopala Krishnan , T. Kalaiarasi , R. Subramaniyan , J. Comp. Methods Phys. (2014) 623235 .

[33] A.D. Becke , K.E. Edgecombe , J. Chem. Phys. 92 (1990) 5397–5403 .

[34] C. A. Lipinski, Lead-and drug-like compounds: the rule-of-five revolution, Drug Discov. Technol. 1(4) (2004) 337- 341, https://doi.org/10.1016/j.ddtec.2004.11.007.
[35] D.E. Pires, T.L. Blundell, D.B. Ascher, pk CSM: Predicting Small-Molecule Pharmacokinetic and Toxicity Properties Using Graph-Based Signatures, J. Med. Chem. 58 (2015) 4066-4072. https://doi.org/10.1021/acs.jmedchem.5b00104